

# Photon yields from nitrogen gas and dry air excited by electrons

M. Nagano <sup>a</sup>, K. Kobayakawa <sup>b</sup>, N. Sakaki <sup>c</sup> and K. Ando <sup>d</sup>

<sup>a</sup>*Department of Space Communication Engineering, Fukui University of Technology, Fukui, 910-8505 Japan*

<sup>b</sup>*Department of Architecture and Civil Engineering, Fukui University of Technology, Fukui, 910-8505 Japan*

<sup>c</sup>*RIKEN (The Institute of Physical and Chemical Research), Wako, 351-0198 Japan*

<sup>d</sup>*Department of Applied Physics and Chemistry, Fukui University of Technology, Fukui, 910-8505 Japan*

---

## Abstract

In order to detect ultrahigh-energy cosmic rays (UHECR), atmospheric fluorescence light from the trajectory of the extensive air shower may be measured by mirror-photosensor systems. In this type of experiment the photon yield from electrons exciting air of various densities and temperatures is most fundamental information for estimating the primary energy of UHECR. An experiment has been undertaken using a  $^{90}\text{Sr}$   $\beta$  source to study the pressure dependence of photon yields, and the life times of the excited states, for radiation in nitrogen and dry air. The photon yield between 300 nm and 406 nm in air excited by 0.85 MeV electrons is  $3.734 \pm 0.148$  ( $\pm 13.2$  % systematic) photons per meter at 1000 hPa and 20 °C. The air density and temperature dependence is given for application to UHECR observations.

*Key words:* nitrogen fluorescence, air fluorescence, extensive air

*PACS:* 96.40.Z, 96.40.Pq, 96.40.De, 32.50.+d

---

## 1 Introduction

The fluorescence technique was first successfully used by the Fly's Eye detector to explore cosmic rays in the ultra-high energy region [1]. From 1998 the HiRes detector, a successor to the Fly's Eye, has been in operation with improved resolution in energy, arrival directions and in measurements of the longitudinal shower development [2]. Fluorescence detectors will be constructed along with

the surface array at the Pierre Auger Observatory [3] and one of them is now in operation in Malargue, Argentina. In these experiments an atmosphere of quite low vapour pressure (i.e. dry) is used as a vast scintillator. In contrast, in the case of a satellite-based telescope viewing downward (EUSO) [4], fluorescence light from extensive air showers is observed mainly over the ocean where air is not dry.

While the fluorescence efficiencies of electrons in the troposphere are fundamentally important, there are only a few measurements which can be applied to the UHECR experiments. Bunner summarized in his Ph.D thesis [5] the fluorescence radiation from air and showed that photons from the 2nd positive (2P) band of the nitrogen molecule and the 1st negative (1N) band of the nitrogen ion were significant. Since there are many vibrational states, there are many lines between 300 nm and 400 nm. Photon yields listed in Bunner's thesis are based on those excited by low energy electrons, deuterons and alpha particles stopped in air (i.e. total absorption conditions) and the errors of each experiment are about 30 %. It is important to measure the photon yields excited by electrons in various bands under thin target conditions. In order to apply them to air shower observations, their density and temperature dependencies must be known in each band.

Kakimoto et al. [6] measured photon yields in thin targets and showed that the yields were proportional to the particle energy loss per unit length,  $dE/dx$ , between 1.4 MeV and 1000 MeV. However, their measurements were limited to three main wavelength bands with central wavelengths of 337 nm, 357 nm and 391 nm. The results of Kakimoto et al. are about 20–40 % larger than those summarized by Bunner at these three wavelengths. They also measured the photon yields using the HiRes optical filter which is sensitive in a wide band between 300 and 400 nm. Using this wide band measurement, Kakimoto et al. estimate the absolute values of the lines not individually measured, and they get the values lower than those determined by Bunner.

Given these previous measurements, it is clear that precise measurements at wavelengths other than the three major lines above are required in thin targets, since optical filters between 300 nm and 406 nm are used in most cosmic ray experiments. We measured the photon yields of electrons in dry air with various pressures to apply to the atmosphere in a desert. The photon yields were measured through filters of central wavelengths of 314.7, 337.7, 356.3, 380.9, 391.9 and 400.9 nm and 10 nm bandwidth. Yields in damp air are now under measurement and will be reported in a subsequent paper.

Recently, the HiRes group reported measurements of the energy spectrum of UHECRs [7]. There are significant discrepancies in the energy spectrum at the highest energies as measured by two experiments, HiRes and AGASA (Akeno Giant Air Shower Array) [8]. Using the values in the present measurement,

we discuss their effect on the energy determination of UHECR's by the fluorescence technique.

## 2 Experiment

### 2.1 Experimental arrangement

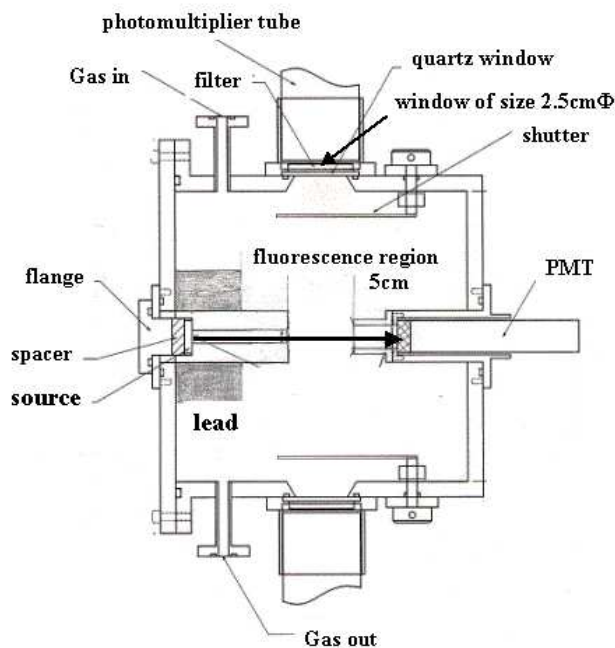


Fig. 1. Schematic drawing of the chamber (top view). Three PMTs are mounted on two sides and the top of the chamber, and they view fluorescence light through quartz windows. Optical filters are mounted between the PMTs and the windows. Electrons from  $^{90}\text{Y} \rightarrow ^{90}\text{Zr}$  are beamed and detected by a scintillation counter.

We chose a photon counting and thin target technique to measure the pressure dependence of photon yields (the number of photons produced by electrons per meter of travel) from nitrogen and air excited by electrons, following the method employed by Kakimoto et al. [6]. The cubic chamber used is shown schematically in Fig. 1. Three photomultiplier tubes of 2 inch diameter (Hamamatsu photon counting H7195PX, named PM1, PM2 and PM3), which were selected for low noise, were mounted on two sides and the top of the chamber, and view the light through quartz windows. A central region (diameter 2.5 cm) of each PMT was used for photon counting. Electrons with a maximum energy of 2.28 MeV from  $\beta$  decay of  $^{90}\text{Sr} \rightarrow ^{90}\text{Y} \rightarrow ^{90}\text{Zr}$  (3.7 MBq) were beamed

by a collimator. The energy of each electron was measured by a scintillation counter (electron counter). The coincidence between the electron counter and any one of the photon counters was used to generate a gate for the ADCs and a start signal for a TDC. A beam length of 5 cm was visible to the three photon counters and the triggered rate of electrons was about  $2.7 \times 10^3 \text{ s}^{-1}$  in vacuum and  $1.5 \times 10^3 \text{ s}^{-1}$  at 1000 hPa. The electron energy was reduced by about 0.17 MeV by a mylar window and the aluminum cover of the source.

The energy spectrum of the triggered electrons is shown in Fig. 2. As seen there, the measured spectrum fits well to the expected decay spectrum of  $\beta$  rays depicted by the solid curve. The threshold and average electron energies are 0.3 and 0.85 MeV respectively. The average energies below and above 0.85 MeV are 0.55 MeV and 1.2 MeV, respectively. The difference in photon yields between these two energy regions will also be presented.

In the present measurements, six narrow band interference filters with central wavelengths of 314.7, 337.7, 356.3, 380.9, 391.9 and 400.9 nm were used. The bandwidth of each filter was about 10 nm. Fig. 3 shows the transmission coefficients of the adopted filters as a function of wavelength (provided by the manufacturer, Hi-Technology Inc). Vertical lines show the relative photon yields of fluorescence lines in air at 1000 hPa listed by Bunner [5], where solid and dotted lines correspond to the yield from 2P and 1N bands, respectively. There remain some lines which are not covered in the present experiment, but their contribution to the total yield may be less than 5 %.

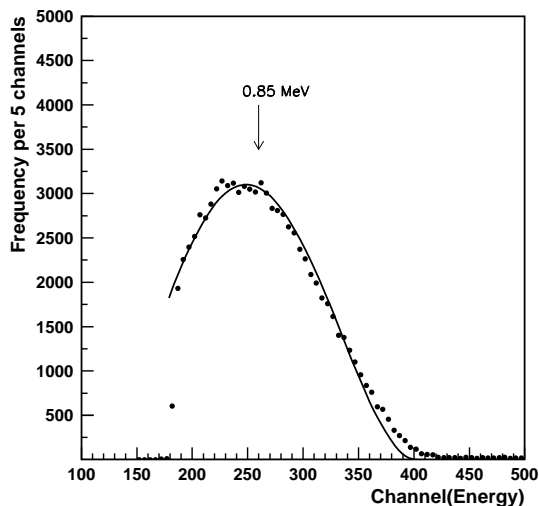


Fig. 2. Energy spectrum of the electrons. Dots represent the observed spectrum and the solid curve is that expected from the  $\beta$  decay of  $^{90}\text{Y}$ . The threshold and average electron energies are 0.3 MeV and 0.85 MeV respectively.

In any one run under a particular set of conditions, the number of incident

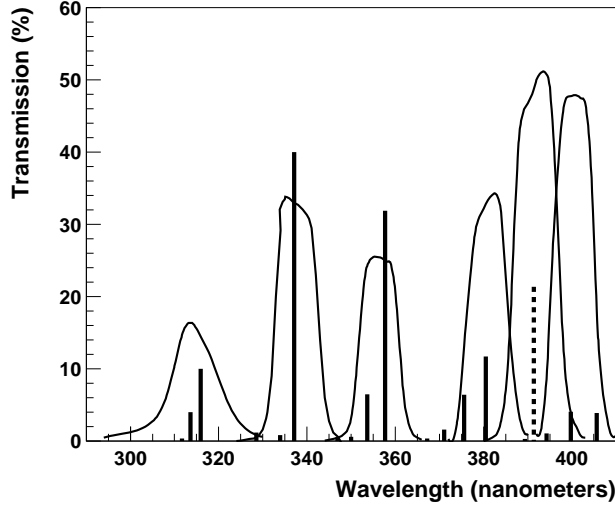


Fig. 3. Transmission coefficients of interference filters used in the present experiment. The relative intensities of fluorescence lines at 1000 hPa from the nitrogen molecule (solid lines) and ion (dotted line) in air from Bunner [5] are also shown neglecting their spectral widths.

electrons at the electron counter was registered. If there was a coincidence in 150 ns between the electron counter and any one of three photon counters, the ADC values of the electron counter and the corresponding photon counter were recorded. The time difference between the photon signal and the electron signal (which was delayed by 180 ns) was also recorded by the TDC in units of 0.5 ns.

Examples of the ADC and TDC distributions are shown in Fig. 4. The coincident time of the electron counter and the photon counter is shown as the 369th channel of the TDC. Since the TDC is started by the photon signal and stopped by the electron signal (delayed by 180 ns), the more the channel decreases the more the photon signal is delayed. The time resolution of the system is measured by using coincident signals of cosmic ray muons between PM2 at the top of the chamber and the electron counter, and is found to be 1.26 ns (3 channels). Signal can clearly be separated from the background in the TDC distribution. Signals above the 369th channel in the lower plot of Fig. 4 are due to background photon signals prior to the electron signal, which were triggered due to the 20 ns pulse width of the discriminator output.

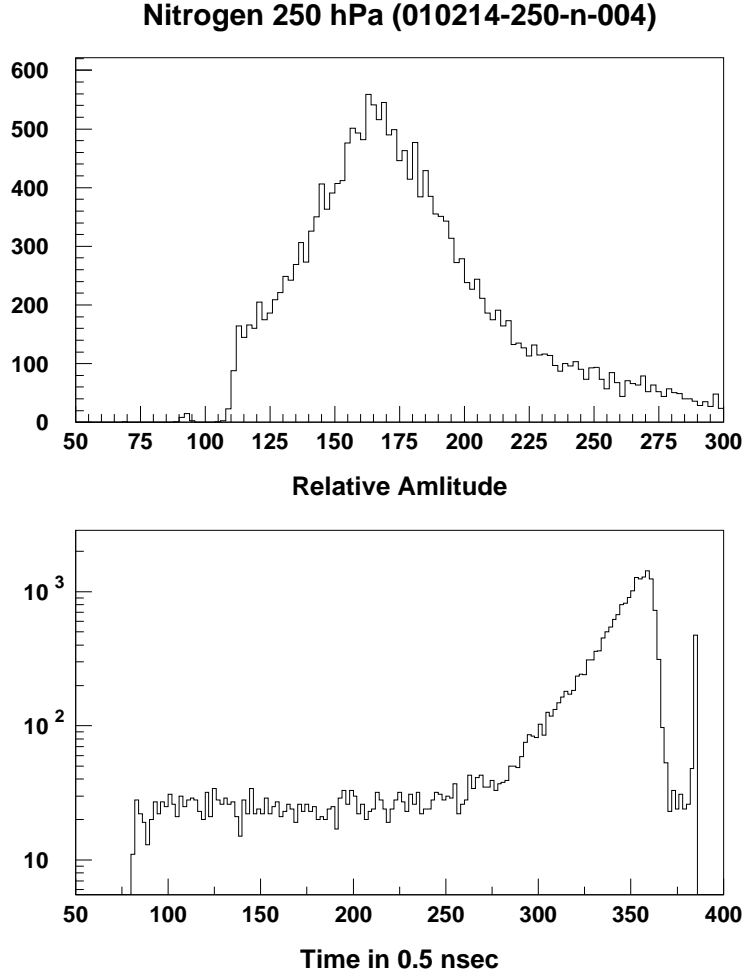


Fig. 4. An example of ADC and TDC distributions (for 250 hPa, N<sub>2</sub>). The upper plot is a typical single photon pulse height distribution and the lower plot shows the time difference between incident electrons and emitted photons. Each channel corresponds to 0.5 ns. The TDC is started by the photon signal and is stopped by the electron signal which is delayed by 180 ns.

## 2.2 Backgrounds

There is a background of single photon PMT noise, which is uniformly distributed in the TDC distribution as shown in Fig. 4. With a shutter was placed in front of each photon counter inside the chamber, some signals were observed even in vacuum runs when a lead brick was not set around the source in Fig. 1. Their rates in the vacuum are listed in Table 1. There are coincident muons measured by the photon counter at the top of the chamber (PM2) and

Table 1

Background rate per minute for the three PMTs in the signal portion of the TDC distribution. These values are for an evacuated chamber when the source was not surrounded by the lead brick. “Port” refers to the position of the PMTs around the chamber.

PMT	port	counting rate per min	rate per min after muon subtraction
PM1	side	$0.0824 \pm 0.0056$	$0.0824 \pm 0.0056$
PM2	top	$0.2154 \pm 0.0091$	$0.0824 \pm 0.0121$
PM3	side	$0.0778 \pm 0.0055$	$0.0778 \pm 0.0055$

the electron counter. This rate is measured to be  $(0.133 \pm 0.008) \text{ min}^{-1}$ . The background after subtraction of muons for PM2 was about 0.08 per minute, as shown in Table 1. The remaining background rate of  $\sim 0.08 \text{ min}^{-1}$  can, according to our calculations, be wholly attributed to Bremsstrahlung photons from the aluminum foil (0.1 mm thickness) of the source window.

In our past report at the 27th ICRC [9], the number of signal counts was obtained by subtracting backgrounds determined from the TDC distribution measured in vacuum. In the present experiment, these backgrounds are reduced to be negligibly small by covering the source region with a lead brick of 5 cm thickness as shown in Fig. 1.

The differences of past measurements (M1) [9] and the present ones (M2) are summarized as follows;

- (1) The visible beam length was shortened from 10 cm to 5 cm, so that the average photon incident angle was reduced from  $9.3^\circ$  to  $5.2^\circ$ . Though we corrected the interference filter transmission coefficients for these photon incident angles in M1, the correction has not been applied to M2.
- (2) The background from Bremsstrahlung photons around the source region in M1 were tabulated, while such a background has been reduced by about  $\frac{1}{8}$  with the 5 cm thick lead brick around the source in M2.

### 2.3 Systematic errors

The systematic errors of the present experiment are summarized in Table 2. The main uncertainty is due to the PMT calibrations (quantum efficiency QE and collection efficiency CE), which were provided by the manufacturer (Hamamatsu Photonics). The filter transmission coefficients are provided by the manufacturer (Hi-Technology Inc.) and the error is mainly due to the various incident angles of the photons at the filter. The error due to a possible contamination of some lines which fall in the tail of a filter’s transmission is listed in the fourth line. The total systematic error is estimated to be 13.2 %,

assuming the errors add in quadrature. The statistical error in each run is less than 3 %.

Table 2

Systematic errors of the present experiment

No.	item	errors
1.	Quantum efficiency of PMT	5 %
2.	Collection efficiency of PMT	10 %
3.	Transmission coefficient of filter	5 %
4.	Contamination from lines at the tail of filter transmission	5 %
	Total	13.2 %

### 3 Results

The number of signal counts was obtained by subtracting backgrounds determined from the background portion of the TDC distribution. This background portion can be discriminated from the signal portion as shown in Fig. 4. The photon yield per unit length per electron  $\epsilon$ , is determined as the number of signal counts  $N$  divided by the product of the following: the total number of electrons  $I$ , the length of the fluorescence portion  $a$ , the solid angle of the PMT  $\Omega$ , the quartz window transmission  $\eta$ , and the filter transmission  $f$ .

$$\epsilon = \frac{N}{I \times a \times \Omega \times \eta \times f \times \text{QE} \times \text{CE}} . \quad (1)$$

In the following analysis we use a value of  $f$  appropriate for the main line in each filter band pass. The effect of another line in one filter will be discussed later.  $I$  is about  $5 \times 10^8$  from about 80 hours in each run.

#### 3.1 Nitrogen

As a first step we have measured  $\epsilon$  in nitrogen, so that we may compare results with previous experiments. The pressure dependencies of  $\epsilon$  in six wave bands are indicated by solid circles in Fig. 5. In each figure, the main line in each filter band is indicated. The results of Kakimoto et al. (cited from Ueno [11]) are also plotted with open squares in the 337 nm and 358 nm bands. The present results at 337 nm and 358 nm are in good agreement with those by Kakimoto et al., even though the PMTs, filters and gas chambers are different in the two experiments.



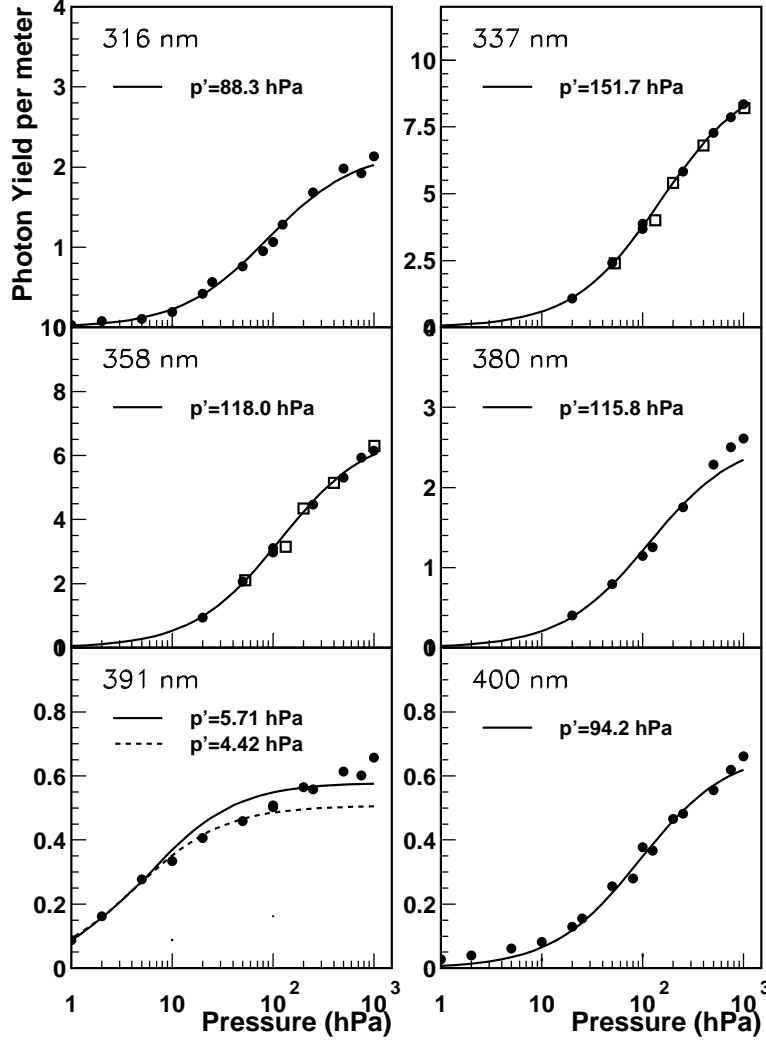


Fig. 5. The pressure dependence of  $\epsilon$  in  $N_2$  at  $17^\circ C$  excited by electrons with an average energy of 0.85 MeV in six wave bands. In each figure, the main contributing line in each wave band is listed. Solid circles are the present results. Open squares are from Kakimoto et al. cited from Ueno [11]. Solid curves are the best fits of Eq.(10) with  $p'$  as shown, discussed below in Section 4.1. The dotted line for the 391 nm band shows the best fit when the five highest points are excluded.

The solid lines in the figure are from Eq.(10), which will be discussed in Section 4.1. A dotted line in the plot for the 391 nm band is the best fit to the equation with the five highest pressure points excluded. The experimental points in some filters cannot be fitted with a constant  $p'$  throughout the pressure range, especially in the 391 nm band. This may be due to the superposition of two lines in one filter band, as will be discussed in Section 4.3.

### 3.2 Air

We used a mixture of 78.8 % nitrogen gas and 21.2 % oxygen gas, without Argon and the other small contributions to air, such as CO<sub>2</sub>, Ne, CO, water vapour etc. This air-like mixture is expected to give similar photon yields to dry air, since the change of photon yields may be negligibly small even if Argon of 1 % is included [5]. In Kakimoto et al, a mixture of nitrogen and oxygen gas was also used as dry air.

The pressure dependence of  $\epsilon$  in dry air is shown in Fig. 6 by filled circles in six wave bands. The results of Kakimoto et al. [6] are also shown by open squares in the 337 nm, 358 nm and 391 nm bands. Their results are larger than the present ones by about 0.1 photons/m irrespective of the pressure, and in all three bands. This is understood as follows: there were backgrounds of photons from Bremsstrahlung at the foil of the source window in Kakimoto et al., while those photons were reduced by a lead brick in this experiment. The effects of this background were negligibly small in the nitrogen measurements as shown in Fig. 5. The solid lines come from Eq.(10), which will be discussed in Section 4.2.

## 4 Analysis and Discussion

### 4.1 Fluorescence decay time and efficiency in N<sub>2</sub> gas

The observed decay time  $\tau$  of the fluorescence is related to the following three terms: the mean lifetime of the excited state for decay to any lower state  $\tau_r$ , the lifetime of collisional de-excitation  $\tau_c$  and that of internal quenching  $\tau_i$ . This can be expressed as follows[5],

$$\frac{1}{\tau} = \frac{1}{\tau_r} + \frac{1}{\tau_c} + \frac{1}{\tau_i} = \frac{1}{\tau_o} + \frac{1}{\tau_c}, \quad (2)$$

and

$$\tau_c = \frac{\sqrt{\pi M k T}}{4\sigma_{nn}} \frac{1}{p}, \quad (3)$$

where  $M$  is the N<sub>2</sub> molecular mass,  $k$  is Boltzmann's constant,  $T$  is the gas temperature,  $\sigma_{nn}$  is the cross-section for nitrogen-nitrogen collisional de-excitation

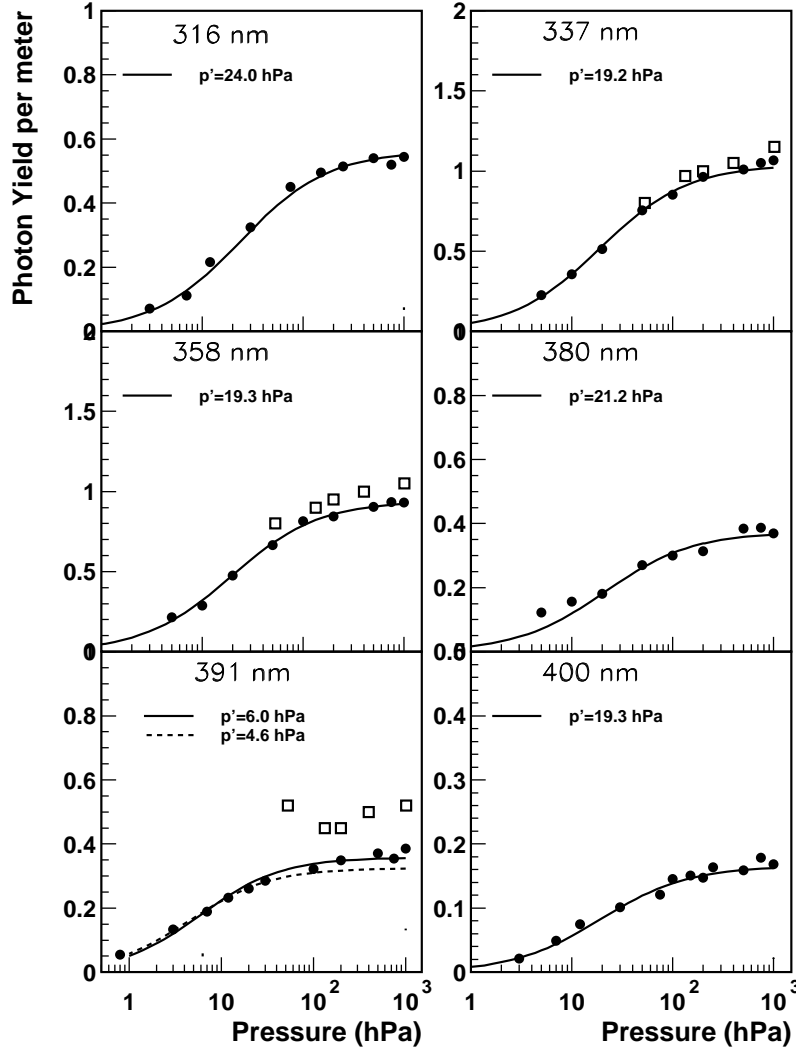


Fig. 6. The pressure dependence of  $\epsilon$  in air at 20 °C. The data of Kakimoto et al. in dry air at 15 °C with 1.4 MeV electrons is plotted by open squares. Solid lines show the best fit of Eq.(10) with the value of  $p'$  as shown, as discussed in Section 4.1. The dotted line in the plot of the 391 nm dependence is the best fit excluding the four highest points.

and  $p$  is the gas pressure. We define the reference pressure  $p'$  [5], which corresponds to the pressure where  $\tau_o$  is equal to  $\tau_c$ , as

$$p' = \frac{\sqrt{\pi M k T}}{4\sigma_{nn}} \frac{1}{\tau_o}. \quad (4)$$

Then the reciprocal of the lifetime  $\frac{1}{\tau}$  is related to  $p$  by

$$\frac{1}{\tau} = \left( \frac{1}{\tau_o p'} \right) p + \frac{1}{\tau_o} = \frac{1}{\tau_o} (ap + 1) , \quad (5)$$

where  $a = \frac{1}{p'}$ .

The fluorescence efficiency of the  $i$ -th band at pressure  $p$ ,  $\Phi_i(p)$ , is defined as the power radiated by the gas in the  $i$ -th band per unit power deposited in the gas by an electron. This  $\Phi_i(p)$  can be written as the ratio of de-excitation by radiation to the total, and is expressed as a function of  $p$  as follows [5]:

$$\Phi_i(p) = \frac{\frac{1}{\tau_r}}{\frac{1}{\tau_o} + \frac{1}{\tau_c}} = \frac{\frac{\tau_o}{\tau_r}}{1 + \frac{\tau_o}{\tau_c}} = \frac{\frac{\tau_o}{\tau_r}}{1 + \frac{p}{p'_i}} . \quad (6)$$

Since the energy available to produce photons in the  $i$ -th band is the electron energy loss per unit length times  $\Phi_i(p)$ , the photon yield per unit length per electron,  $\epsilon_i$ , for  $i$ -th band under atmospheric pressure  $p$  is written as follows [10]:

$$\epsilon_i = \rho \left( \frac{dE}{dx} \right) \left( \frac{\Phi_i(p)}{h\nu_i} \right) , \quad (7)$$

and

$$\Phi_i(p) = \frac{\Phi_i^\circ}{1 + \frac{p}{p'_i}} , \quad (8)$$

where  $\rho$  is the air density ( $\text{kg m}^{-3}$ ),  $\frac{dE}{dx}$  is the energy loss in ( $\text{eV kg}^{-1} \text{ m}^2$ ), and  $h\nu_i$  is the photon energy of the  $i$ -th band ( $\text{eV}$ ).  $\Phi_i^\circ (= \frac{\tau_o}{\tau_r})$  corresponds to the fluorescence efficiency for the  $i$ -th band in the absence of collisional quenching.

By using the equation of state of a gas,  $p = \rho R_{N_2} T$  where  $R_{N_2}$  is the specific gas constant in  $N_2$  ( $296.9 \text{ m}^2 \text{s}^{-2} \text{K}^{-1}$ ), Eq.(7) is rewritten as a function of  $p$  at a constant temperature  $T$  in Kelvin:

$$\epsilon_i = \frac{p}{R_{N_2} T h\nu_i} \left( \frac{dE}{dx} \right) \left( \frac{\Phi_i^\circ}{1 + \frac{p}{p'_i}} \right) \quad (9)$$

$$= \frac{C_i p}{1 + \frac{p}{p'_i}} = \frac{C_i}{x + a_i} . \quad (10)$$

where  $x = \frac{1}{p}$  and  $a_i = \frac{1}{p'_i}$ . This relation can be written in a more general form as a function of the gas density and the temperature as [6]

$$\epsilon_i = \frac{A_i \rho}{1 + \rho B_i \sqrt{T}} , \quad (11)$$

where

$$A_i = \frac{\left(\frac{dE}{dx}\right) \Phi_i^\circ}{h\nu_i} \quad \text{and} \quad B_i = \frac{R_{N_2} \sqrt{T}}{p'_i} = \frac{4\sigma_{nn}\tau_o R_{N_2}}{\sqrt{\pi k M}} . \quad (12)$$

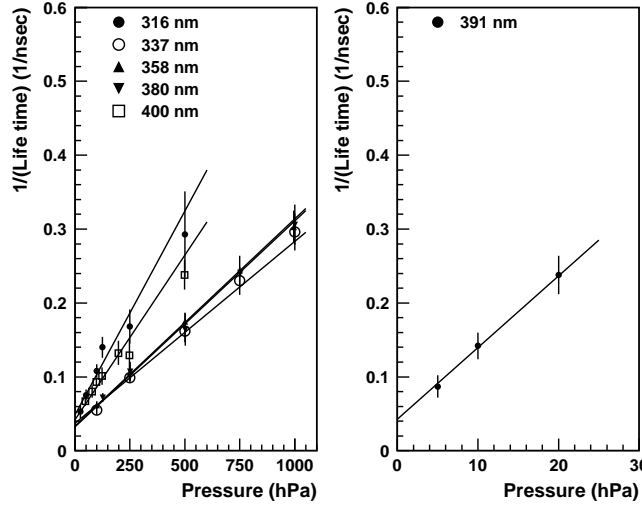


Fig. 7. The pressure dependencies of  $\frac{1}{\tau}$  for the excited states of  $N_2$  for 6 wave bands.

The pressure dependencies of  $\frac{1}{\tau}$  for various wave bands in  $N_2$  are shown in Fig. 7. In order to fit the experimental points of Fig. 5 and 7 to Eq.(10) and (5) respectively, the least square (LS) method is utilized. Let us consider first the fit to the  $p - \epsilon$  diagram (Fig. 5), since the data points are more numerous than those in  $p - \frac{1}{\tau}$  diagram. For each  $i$ -th band the first  $\chi_1^2$  is defined by

$$\chi_1^2 = \sum_j \omega_j \left( \epsilon_j - \frac{C}{x_j + a} \right)^2 . \quad (13)$$

where the weights  $\omega_j$  come from the errors in  $\epsilon_j$  at  $p_j (= \frac{1}{x_j})$ . By minimizing  $\chi_1^2$ , we find the first values of  $a^{(1)}$  and  $C^{(1)}$ . Then after linearizing Eq.(10) using  $a^{(1)}$  and  $C^{(1)}$ , Newton's method [13] is applied to estimate the final  $a^{(\nu)}$  and  $C^{(\nu)}$  after the  $\nu$ -th iteration. The statistical errors of  $a^{(\nu)}$  and  $C^{(\nu)}$  are evaluated using the propagation law of errors using those of  $\epsilon_j$ . For a given

$a^{(\nu)}$ , it is easy to find  $\tau_0$  and its error by the LS method because Eq.(5) is linear with respect to  $(ap+1)$ . The obtained results are shown by solid curves in Fig. 5 and by lines in Fig. 7. The parameters are listed in Table 3. The values of  $\sigma_{nn}$  derived from  $\tau_0 p'$  and  $\Phi^\circ$  from  $C$  are also listed in the table. In the case of the 391 nm band, we find that the experimental points do not fit well to one value of  $p'$  throughout the pressure range but a dashed line in Fig. 5 shows Eq.(10) for a limited range of pressures.

Table 3

$\tau_o$ ,  $p'$ ,  $\sigma_{nn}$ ,  $C$  and  $\Phi^\circ$  in N<sub>2</sub>.

wavelength	$\tau_o$	$p'$	$\sigma_{nn}$	$C$	$\Phi^\circ$
nm	ns	hPa	$\times 10^{-20} \text{m}^2$	$\times 10^{-2} / (\text{hPa}\cdot\text{m})$	$\times 10^{-3}$
316	$20.52 \pm 2.21$	$88.28 \pm 7.48$	$3.36 \pm 0.46$	$2.50 \pm 0.13$	$0.509 \pm 0.028$
337	$26.77 \pm 1.35$	$151.75 \pm 4.83$	$1.50 \pm 0.09$	$6.27 \pm 0.13$	$1.195 \pm 0.025$
358	$30.18 \pm 0.60$	$117.99 \pm 3.99$	$1.71 \pm 0.07$	$5.71 \pm 0.13$	$1.027 \pm 0.023$
380	$30.92 \pm 0.58$	$115.85 \pm 11.05$	$1.70 \pm 0.17$	$2.26 \pm 0.10$	$0.382 \pm 0.017$
391	$23.39 \pm 0.63$	$4.42 \pm 0.23$	$58.96 \pm 4.06$	$11.47 \pm 0.52$	$1.897 \pm 0.085$
400	$23.79 \pm 1.81$	$94.21 \pm 7.93$	$2.72 \pm 0.31$	$0.72 \pm 0.04$	$0.116 \pm 0.007$

Table 4

Comparison of  $\Phi_i(p)$  in N<sub>2</sub> at  $p=800$  hPa (600 mmHg). D. and O. refers to Davidson and O'Neil [14].

	This experiment	Ueno	D. & O.
beam	electron	electron	electron
energy	0.85 MeV	1.4 MeV	50 keV
wavelength	$\times 10^{-4}$		
316 nm	$0.505 \pm 0.051$		
337 nm	$1.901 \pm 0.072$	$1.87 \pm 0.01$	5.20
358 nm	$1.320 \pm 0.054$	$1.35 \pm 0.01$	3.70
380 nm	$0.483 \pm 0.051$		1.40
391 nm	$0.104 \pm 0.007$		0.102
400 nm	$0.122 \pm 0.013$		0.200

Our values of  $\Phi_i(p)$  in N<sub>2</sub> at 800 hPa are listed in Table 4, together with those of other experiments. The electron energy loss  $\frac{dE}{dx}$  is calculated using the equation in Sternheimer et al. [15] with a density correction, and is  $0.1687 \text{ MeV/kg}\cdot\text{m}^{-2}$  and  $0.1677 \text{ MeV/kg}\cdot\text{m}^{-2}$  at 0.85 MeV, for N<sub>2</sub> and air respectively. The values from the experiments by Kakimoto et al. are cited from Ueno [11] and agree well with the present ones for the 337 nm and 358 nm bands. However, the

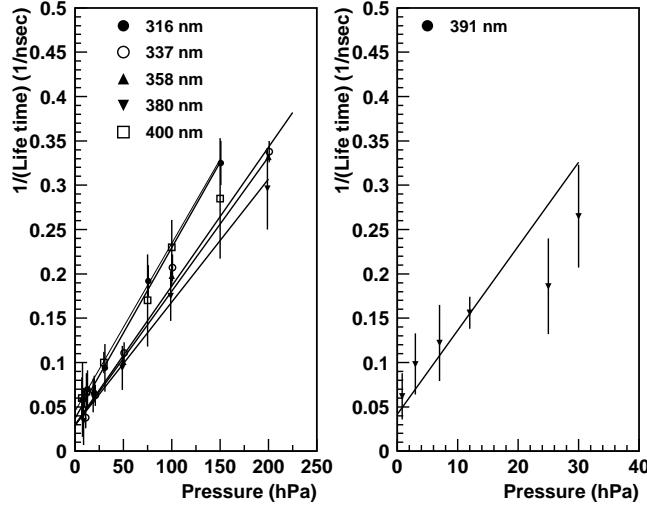


Fig. 8. The pressure dependence of the reciprocal of the fluorescence decay time ( $\frac{1}{\tau}$ ) in air.

values by Davidson & O'Neil [14] are about a factor of 2.8 larger than the present results except at 391 nm and 400 nm.

The present result for  $\Phi_i^\circ$  at 391 nm is  $(1.897 \pm 0.085) \times 10^{-3}$  which does not agree with the result  $(6.0 \pm 1.9) \times 10^{-3}$  by M.N.Hirsh et al. [12], measured using electrons of 1.46 MeV under a gas pressure of less than 10 hPa. This will be discussed in Section 4.3 in connection with the two lines contained within this filter band.

#### 4.2 Fluorescence decay time and efficiency in dry air

In the case of air, the reference pressure  $p'$  of Eq.(4) may be written as [5]:

$$\frac{1}{p'} = \frac{4\tau_o}{\sqrt{\pi M_n k T}} \left( f_n \sigma_{nn} + f_o \sigma_{no} \sqrt{\frac{M_n + M_o}{2M_o}} \right) = \frac{D}{\sqrt{T}}. \quad (14)$$

where  $M_n$  and  $M_o$  are the masses of nitrogen and oxygen molecules, respectively.  $\sigma_{nn}$  and  $\sigma_{no}$  are the cross-sections for collisional loss by excited nitrogen molecules without radiation, through collisions with other nitrogen or oxygen molecules, respectively. The fraction of nitrogen  $f_n$  is 0.79 and that of oxygen  $f_o$  is 0.21.

The pressure dependence of  $\frac{1}{\tau}$  in dry air is shown in Fig. 8 for six wave bands. The fitting of parameters from Eq.(10) and (5) to the data points in Fig.

Table 5  
 $\tau_o$ ,  $p'$ ,  $\sigma_{no}$ ,  $C$  and  $\Phi^\circ$  in air

wavelength	$\tau_o$	$p'$	$\sigma_{no}$	$C$	$\Phi^\circ$
nm	n	hPa	$\times 10^{-19} \text{m}^2$	$\times 10^{-2}/(\text{hPa}\cdot\text{m})$	$\times 10^{-3}$
316	$22.02 \pm 0.54$	$24.04 \pm 1.99$	$4.30 \pm 0.70$	$2.34 \pm 0.14$	$0.463 \pm 0.029$
337	$33.34 \pm 2.04$	$19.16 \pm 0.72$	$4.06 \pm 0.29$	$5.43 \pm 0.15$	$1.006 \pm 0.027$
358	$34.15 \pm 0.43$	$19.33 \pm 1.36$	$3.83 \pm 0.31$	$4.86 \pm 0.27$	$0.850 \pm 0.047$
380	$33.92 \pm 1.59$	$21.24 \pm 2.62$	$3.45 \pm 0.46$	$1.76 \pm 0.18$	$0.289 \pm 0.029$
391	$24.19 \pm 3.20$	$4.61 \pm 0.34$	$3.70 \pm 0.62$	$7.04 \pm 0.39$	$1.131 \pm 0.063$
400	$26.88 \pm 1.92$	$19.32 \pm 1.79$	$4.65 \pm 0.76$	$0.86 \pm 0.06$	$0.134 \pm 0.009$

6 and 8 is done using the same method as described for the  $\text{N}_2$  case. Three parameters,  $a$  (or  $p'$ ),  $C$  and  $\tau_o$  and their errors are thus evaluated. The results are shown by solid curves in Fig. 6 and Fig. 8 and the parameters are listed in Table 5. The cross-section  $\sigma_{no}$  is derived from  $\tau_o p'$ , where  $p'$  is given by Eq.(14) with  $\sigma_{nn}$  determined previously.  $\Phi^\circ$  and  $C$  are also included in the table. In the case of 391 nm, the dashed curve in Fig. 6 represents parameters in Table 5.

Table 6  
Comparison of  $\Phi_i(p)$  in air at  $p=800$  hPa

	This experiment	Kakimoto	D. & O.	Hartman	Bunner
beam	electron	electron	electron	electron	$\alpha$
energy	0.85 MeV	1.4 MeV	50 keV		4 MeV
nm	$\times 10^{-6}$				
316	$13.12 \pm 1.36$			3.0	5.3
337	$23.69 \pm 1.09$	21	$21.0 \pm 3.2$	20.0	8.5
358	$20.20 \pm 1.80$	22	$15.0 \pm 2.3$	16.0	5.8
380	$7.53 \pm 1.19$		$5.2 \pm 0.8$		4.1
391	$6.48 \pm 0.60$	8.4	$7.0 \pm 1.1$	5.9	4.8
400	$3.18 \pm 0.36$		$1.8 \pm 0.3$	1.7	1.5

The yield in air  $\epsilon_i$  is expressed by Eq.(11), after replacing  $R_{\text{N}_2}$  by  $R_{\text{air}}=287.1 \text{ m}^2\text{s}^{-2}\text{K}^{-1}$  and by using  $p'_i$  given by Eq.(14). The values of  $\Phi_i(p)$  in air at 800 hPa are listed in Table 6 together with results of other experiments. Those of Hartman and Bunner are calculated by using  $\Phi_i^\circ$  and  $p'$  listed in Table 2.6 of Bunner [5]. These values of  $\Phi_i(p)$  at  $p=800$  hPa are in good agreement, except those of Bunner which were measured using alpha beams.



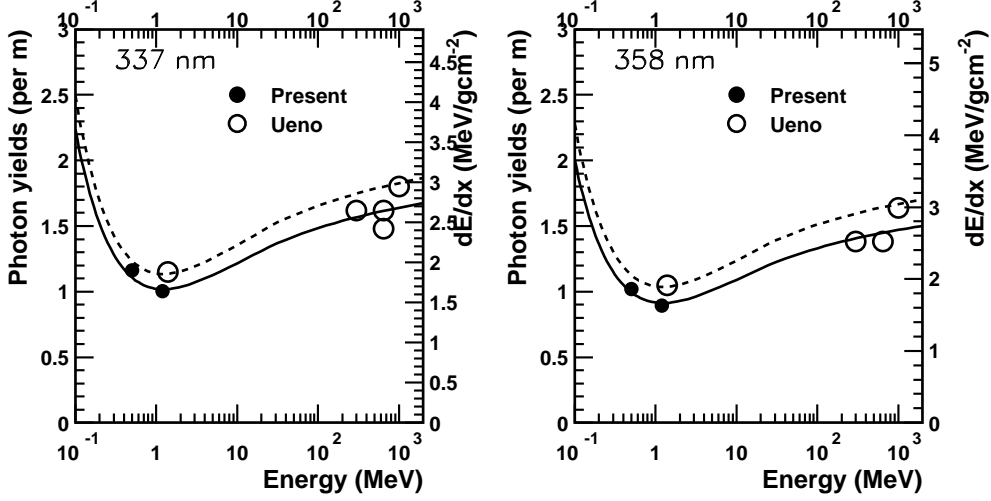


Fig. 9. Energy dependence of  $\epsilon$  in air at 1000 hPa. The  $dE/dx$  curve is shown by a solid line, and is normalized to the yield at 1.2 MeV (present measurement).

In order to see the energy dependence of  $\epsilon_i$  in air, values of  $\epsilon_i$  are derived in two energy regions below and above the average energy (0.85 MeV). In Fig. 9, the energy dependence of  $\epsilon_i$  in air at 1000 hPa is shown for two wave bands together with measurements by Kakimoto et al. cited from the thesis of Ueno [11]. The  $\frac{dE}{dx}$  of an electron in air is calculated from a formula given in Sternheimer et al.[15] and the solid line is normalized to the 1.2 MeV yield point of the present measurements. A dashed line is normalized to the 1.4 MeV point of Ueno in each figure. The solid lines agree with the higher energy measurements (between 300 MeV and 1000 MeV) better than the dashed lines. This may be because the photon backgrounds were not excluded from the 1.4 MeV points of Ueno, as described in Section 3.2. It may be accepted that  $\epsilon$  is proportional to  $\frac{dE}{dx}$ .

#### 4.3 Two components analysis in one filter band

There are some discrepancies between the experimental points and the model pressure dependencies of  $\frac{1}{\tau_i}$  and  $\epsilon_i$  as shown in Eqs.(5) and (10), especially in the 391 nm filter band. In the following, we try to fit the observed pressure dependencies of  $\frac{1}{\tau_i}$  and  $\epsilon_i$  with a superposition of two lines in one filter band. In this case the observed photon yield  $\epsilon_{\text{obs}}(p)$  is the sum of the photon yields of the main line  $\epsilon_1(p)$  and the sub-line  $\epsilon_2(p)$ , and is written as follows by extending Eq.(10):

$$\epsilon_{\text{obs}}(p) = \epsilon_1(p) + \epsilon_2(p) = \frac{C_1}{x + a_1} + \frac{C_2}{x + a_2} , \quad (15)$$

where  $x = \frac{1}{p}$ ,  $a_1 = \frac{1}{p'_1}$  and  $a_2 = \frac{1}{p'_2}$ .  $C_1$  and  $p'_1$  are the parameters of the main line in the filter band, and  $C_2$  and  $p'_2$  are the parameters of another line. It should be noted that  $\epsilon_{\text{obs}}$  is determined assuming the filter transmission of the main line in the filter, and hence  $\epsilon_2$  must be corrected with using the filter transmission of that line.

The reciprocal of the observed life time  $\frac{1}{\tau_{\text{obs}}(p)}$  is approximately expressed by the weighted mean of  $\frac{1}{\tau_1(p)}$  and  $\frac{1}{\tau_2(p)}$ . The weights are expressed in terms of the relative photon intensities of two lines. Therefore,

$$\frac{1}{\tau_{\text{obs}}(p)} = \left( \frac{\epsilon_1(p)}{\epsilon_1(p) + \epsilon_2(p)} \right) \frac{1}{\tau_1(p)} + \left( \frac{\epsilon_2(p)}{\epsilon_1(p) + \epsilon_2(p)} \right) \frac{1}{\tau_2(p)} , \quad (16)$$

where

$$\begin{aligned} \frac{1}{\tau_1(p)} &= \frac{1}{\tau_{o1}}(a_1 p + 1) , \\ \frac{1}{\tau_2(p)} &= \frac{1}{\tau_{o2}}(a_2 p + 1) . \end{aligned} \quad (17)$$

In this case, we have to determine a set of four parameters  $a_1$ ,  $C_1$ ,  $a_2$  and  $C_2$  in Eq.(15). For many such sets, the value of  $\chi^2$  is computed and the set having the minimum  $\chi^2$  is taken as the initial set. Newton's method is also applied for this set, which leads to the final set after the  $\nu$ -th iteration. Values of  $a_1(= \frac{1}{p'_1})$ ,  $C_1$ ,  $a_2(= \frac{1}{p'_2})$  and  $C_2$  determined in this way are listed in the upper half of Tables 7 and 8.

The errors of these four parameters (as listed in the tables) are estimated in the following way. Since the probability density function (pdf) of  $\Delta\chi^2$ , i.e. the deviation from  $\chi^2_{\text{min}}$ , follows the pdf of  $\chi^2$  with four degrees of freedom, we take  $\Delta\chi^2_{\text{critical}}=4.72$  where the coverage probability is 0.683 corresponding to the 1-sigma [18]. Many sets of  $(p'_1, C'_1, p'_2, C'_2)$  near to  $(p'_1, C_1, p'_2, C_2)$  are selected such that the value of  $\chi^2$  almost equals  $\chi^2_{\text{min}} + \Delta\chi^2_{\text{critical}}$ . The maximum and minimum values of  $(p'_1 - p'_1)$  lead to the error bounds of  $p'_1$ . Errors of other three parameters are estimated in the same way.

The best fit result for a superposition of two lines in the 391 nm band of  $\text{N}_2$  is shown in the upper figure of Fig. 10, where the contribution from the main line is shown as a dashed curve and that from the second line is shown as a dotted curve. The solid curve in the left-hand figure is the sum of the dashed and dotted lines, while the solid line in the right-hand figure is the weighted

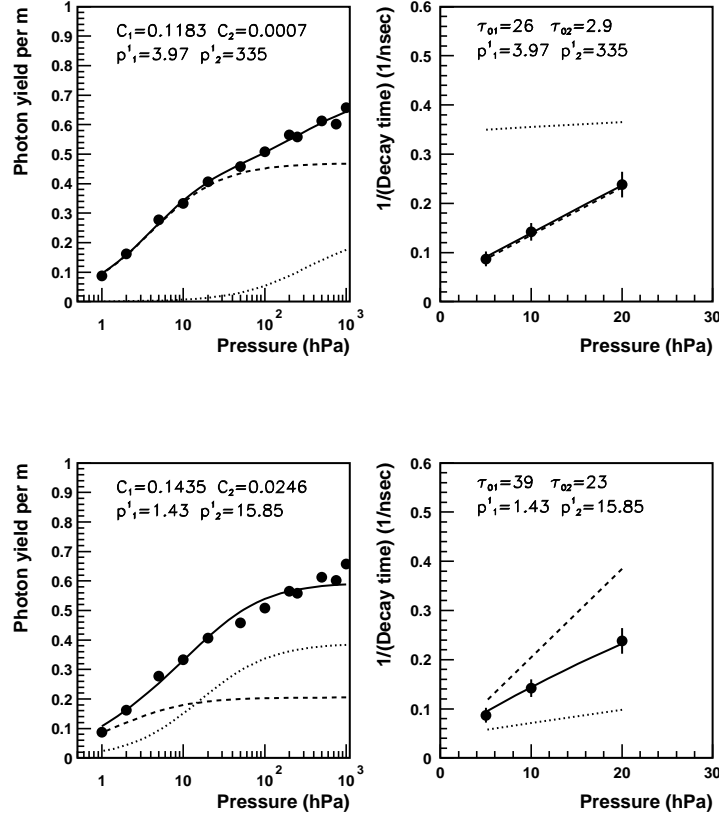


Fig. 10. Two line fitting for the 391 nm bands in  $N_2$ . The upper figure is the best fit combination of two lines. The lower figure is the best fit for a fixed  $p'_1$ . The contribution from the main line is shown by a dashed curve, and the secondary line by a dotted curve. The solid curves are the sum of two lines in the left-hand figures and the weighted sum of two lines expressed by Eq.(16) in the right-hand figures.

Table 7

Parameters of two line fitting in the 391 nm band of  $N_2$ .

Wave length	$p'$	$\tau_0$	$C$	$\Phi^\circ$	$\chi^2$
nm	hPa	ns	$\times 10^{-2}/(\text{hPa}\cdot\text{m})$	$10^{-3}$	
391	$3.97 \pm 0.37$	26.0	$11.83 \pm 0.67$	$1.943 \pm 0.110$	32.7
394	$335. \begin{smallmatrix} +242 \\ -102 \end{smallmatrix}$	2.9	$0.071 \pm 0.028$	$0.012 \pm 0.005$	
391	1.43	39.0	$14.35 \pm 2.50$	$2.357 \pm 0.411$	162.2
394	$15.85 \pm 5.28$	23.0	$2.47 \pm 0.87$	$0.403 \pm 0.142$	

mean of two lines as expressed by Eq.(16). The parameters of each line are listed in Table 7.

It is clear that the fitting is much better than the single line fitting in Fig. 5.

However, the value of  $\Phi^\circ$  at 391 nm is much smaller than the measurement of Hirsh et al.[12], which was determined using 1.45 MeV electrons in the pressure range between 0 and 10 hPa. If we fit their pressure dependence of photon yields with Eq.(10) and with fixed  $p'_1=1.43$  hPa, the best fit case is shown in the lower half of Fig. 10 and the parameters are listed in the lower half of Table 7. The agreement of  $\Phi^\circ$  at 391 nm with Hirsh et al. is better than our best fit case, but the difference is still beyond the measurement errors of both experiments. To resolve the issue, we need to measure the yields at 391 nm with a narrower bandwidth filter.

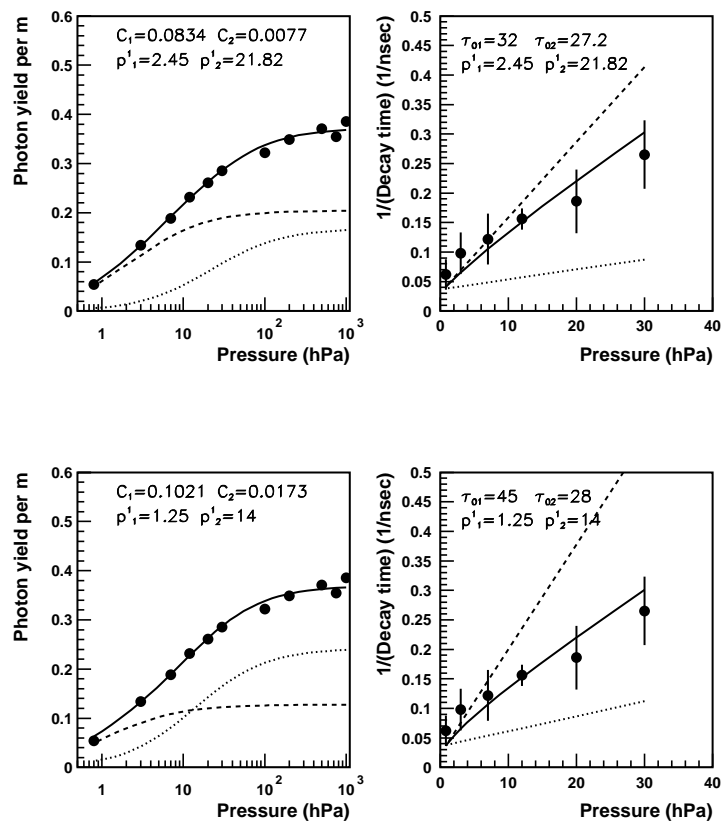


Fig. 11. Two line fitting of the 391 nm band in air. The upper figure shows the best fit to a combination of two lines. The lower one is the best fit with a fixed  $p'_1$ . The contribution from the main line is indicated by a dashed curve, with the second line contribution indicated by a dotted line. Solid curves are the sum of the two lines in left-hand figures, and the weighted sum of two lines (as expressed by Eq.(16)) in the right-hand figures.

In the case of the 391 nm band in air, two cases are also shown in Fig. 11. As before, the first shows the best fit combination of two lines, allowing freedom in the pressure dependence of each line. The second set of plots shows the case where we use a fixed value of  $p'_1$  as determined by Hirsh et al.[12].

Table 8

Parameters of two line fitting in the 391 nm band in air.

Wave length	$p'$	$\tau_0$	$C$	$\Phi^\circ$	$\chi^2$
nm	hPa	ns	$\times 10^{-2}/(\text{hPa}\cdot\text{m})$	$10^{-3}$	
391	$2.45 \pm 0.85$	32.0	$8.34 \pm 1.44$	$1.332 \pm 0.230$	26.82
394	$21.8 \pm 8.5$	27.2	$0.77 \pm 0.33$	$0.122 \pm 0.052$	
391	1.25	45.0	$10.21 \pm 1.35$	$1.631 \pm 0.216$	32.09
394	$13.99 \pm 2.55$	28.0	$1.73 \pm 0.40$	$0.274 \pm 0.063$	

In the other filter bands we have also determined the best fit  $p'$  and  $\tau_0$  values for two lines in a filter band. However, the best fit values of  $p'$  are quite different in some cases for the 337 nm, 356 nm, 380 nm and 400 nm bands, where lines of the  $2P(0, v'')$  and  $2P(1, v'')$  transitions are superimposed. We have decided not to list the values in this article and we continue the experiments with a narrower band width and improvements of the analysis method.

In Table 9, we summarize the present results for electrons of average energies of 0.85 MeV at 1000 hPa. Fitted values of  $\epsilon$  in the 4th column correspond to photons in each filter band, assuming only one line in each band, and assuming a filter transmission at the wavelength of the main line. The exception is the 391 nm filter, where  $\epsilon$  is separated into two lines. The values in parentheses with upper suffix <sup>a</sup> in column 4 are not measured in this experiment but are estimated as follows. The average ratio of our measured values in other wave bands to the corresponding values listed in Bunner [5] is determined, and this ratio is multiplied by the yields in Bunner. In the case of the filters with central values of 380.9 nm and 400.9 nm, the transmission coefficients for the 375.6 nm and 405.9 nm lines are low compared to the values used and the photon yields corrected for transmission coefficients of these lines are listed in parentheses and denoted by an upper suffix <sup>b</sup>. The sum of the measured and corrected values are listed at the bottom of column 4.

Values of  $\Phi^\circ$  calculated from Eq.(10) are listed in the 5th column. In order to apply the present measurements to air shower fluorescence experiments, the fluorescence yields per meter per electron must be known as a function of air density and the temperature for each wavelength.  $A_i$  and  $B_i$  from Eq.(11) are listed in the 6th and 7th column.

The total photon yield between 300 nm and 406 nm given by Bunner is about 14 % smaller than the present corrected results. His value was obtained as weighted averages of three measurements by Davidson and O'Neil (50 keV electrons) [14], Hartman (electrons, cited from [5]) and Bunner (alpha particles) [5], and the accuracy of each of the three experiments was not better than  $\pm 30$  % [5]. Therefore the disagreement may be within their measurement

Table 9

Summary of the present experiments. Photon yields ( $\epsilon$ ) per meter per electron of average energy 0.85 MeV are values in dry air at 1000 hPa and 20 °C. Values in parentheses with an upper suffix <sup>a</sup> have not been measured in this experiment and are estimated as described in the text. Values in parentheses with an upper suffix <sup>b</sup> are corrected values taking into account the transmission coefficient (see text for detail).

i	$\lambda$	transition	$\epsilon$	$\Phi^\circ$	$A$	$B$
	nm	state	m <sup>-1</sup>	$\times 10^{-3}$	m <sup>2</sup> kg <sup>-1</sup>	m <sup>3</sup> kg <sup>-1</sup> K <sup>−<math>\frac{1}{2}</math></sup>
1	311.7	2P(3,2)	0.552±0.033	0.463±0.029	19.59±1.20	2.04±0.17
2	313.6	2P(2,1)				
3	315.9	2P(1,0)				
4	328.5	2P(3,3)	(0.041±0.012) <sup>a</sup>			
5	330.9	2P(2,2)				
6	333.9	2P(1,1)				
7	337.1	2P(0,0)	1.024±0.028	1.006±0.027	45.42±1.23	2.56±0.09
8	346.9	2P(3,4)	(0.030±0.009) <sup>a</sup>			
9	350.0	2P(2,3)				
10	353.7	2P(1,2)				
11	357.7	2P(0,1)	0.926±0.051	0.850±0.047	40.71±2.27	2.54±0.18
12	367.2	2P(3,5)	(0.054±0.016) <sup>a</sup>			
13	371.1	2P(2,4)				
14	375.6	2P(1,3)				
15	380.5	2P(0,2)	0.367±0.038	0.289±0.029	14.71±1.49	2.31±0.25
17	391.4	1N(0,0)	0.204±0.079	1.331±0.230	69.77±12.2	20.07±6.92
16	389.4	2P(3,6)	0.163±0.071	0.121±0.052	6.40±2.78	2.25±0.09
18	394.3	2P(2,5)				
19	399.8	2P(1,4)				
20	405.9	2P(0,3)	(0.247±0.043) <sup>b</sup>	(0.205±0.035) <sup>b</sup>	(10.86±1.89) <sup>b</sup>	
Sum(measured)			3.399±0.132			
Sum(corrected)			3.734±0.148			

errors.

#### 4.4 Effect of the present results to the energy estimation of UHECR

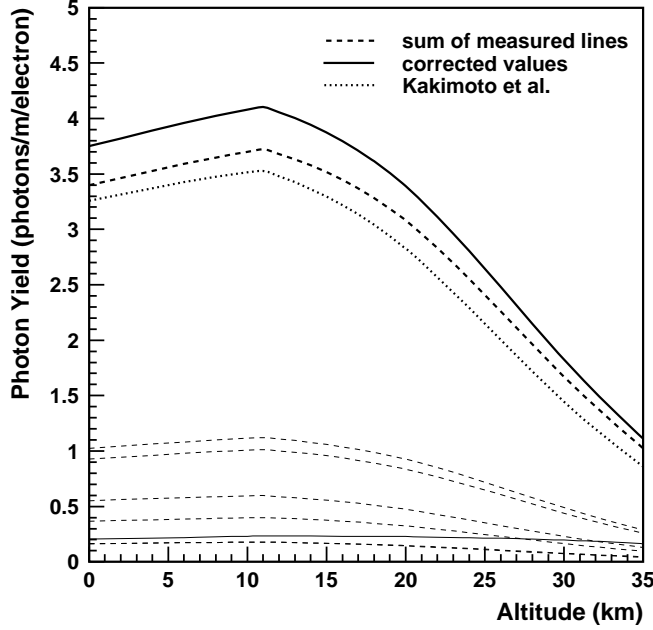


Fig. 12. Photon yield between 300 and 406 nm for a 0.85 MeV electron as a function of altitude. The US Standard Atmosphere 1976 [19] is used for the atmospheric model. The thin solid line is the altitude dependence of the 391 nm line and the thin dashed lines are those of other lines. The heavy dashed line is the sum of all measured lines. A heavy solid line represents the corrected values for the unmeasured contributions. The dotted heavy line is the photon yield between 300 nm and 400 nm from Kakimoto et al., calculated for a 0.85 MeV electron using their equation.

In Fig. 12, the photon yield between 300 nm and 406 nm for a 0.85 MeV electron is shown as a function of altitude. The US Standard Atmosphere 1976 [19] is assumed. The thin solid line is the altitude dependence of the 391 nm line and the thin dashed lines are those of the other lines listed in Table 9. The heavy dashed line is the sum of all measured lines. It should be noted that the altitude dependence is almost the same for all 2P lines. The yield from the 391 nm line is, however, almost independent of altitude, but its proportion increases with altitude. The heavy solid line is the corrected one described in the previous section. As done by Kakimoto et al., the total photon yields between 300 nm and 406 nm can be approximated as a superposition of two sets of terms, for the 2P lines and the 1N line, as follows:

$$\epsilon = \frac{\left(\frac{dE}{dx}\right)}{\left(\frac{dE}{dx}\right)_{0.85\text{MeV}}} \times \rho \left( \frac{A_1}{1 + \rho B_1 \sqrt{T}} + \frac{A_2}{1 + \rho B_2 \sqrt{T}} \right), \quad (18)$$

where  $\rho$  is the air density in  $\text{kg m}^{-3}$  and  $T$  is in Kelvin (K). Our values are  $A_1 = 147.4 \pm 4.3 \text{ m}^2\text{kg}^{-1}$ ,  $A_2 = 69.8 \pm 12.2 \text{ m}^2\text{kg}^{-1}$ ,  $B_1 = 2.40 \pm 0.18 \text{ m}^3\text{kg}^{-1}\text{K}^{-1/2}$ ,  $B_2 = 20.1 \pm 6.9 \text{ m}^3\text{kg}^{-1}\text{K}^{-1/2}$ . Here the energy loss  $\frac{dE}{dx}$  is normalized at 0.85 MeV. Though the parameters  $A_1$ ,  $A_2$ ,  $B_1$  and  $B_2$  from Kakimoto et al. [6] are different from the present results, their altitude dependence is quite similar to the present experiment, as shown by the heavy dotted line in the figure. But the absolute values of the yield are somewhat different.

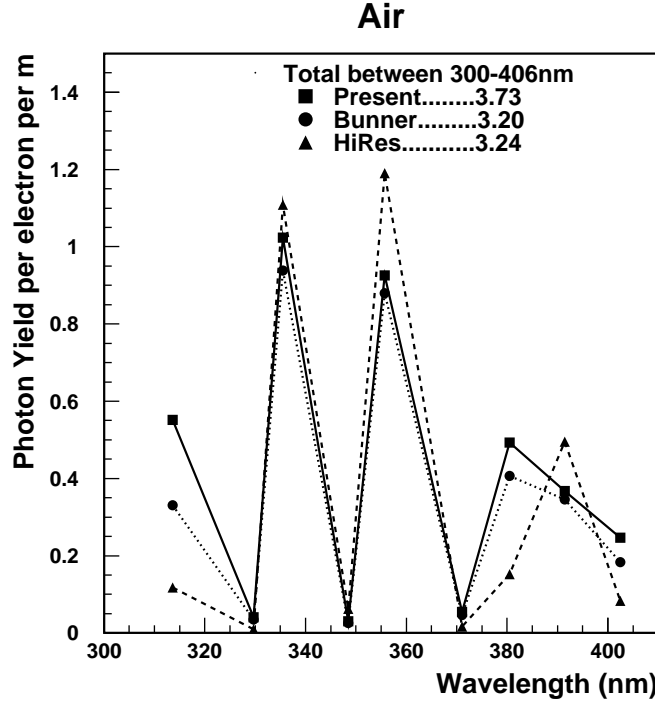


Fig. 13. Comparison of  $\epsilon$  from the present experiment (solid line) with those from Bunner (dotted line) and those used in the HiRes analysis (dashed line).

Fig. 13 shows a comparison of  $\epsilon$  from the present results between 300 nm and 406 nm, with those from Bunner and those values used by the HiRes experiment [17]. For an electron in air,  $(\frac{dE}{dx})_{0.85\text{MeV}} = 0.1677 \text{ MeV/kg}\cdot\text{m}^{-2}$  and  $(\frac{dE}{dx})_{1.4\text{MeV}} = 0.1659 \text{ MeV/kg}\cdot\text{m}^{-2}$  corresponding to ours and the HiRes, respectively. Therefore we may directly compare the present values of yields and those used by them. Though the values used in the HiRes experiment are larger than the present ones in the three main bands (337 nm, 356 nm, 391 nm), the HiRes total number of photons between 300 and 406 nm is about 13 % lower than ours as seen in Fig. 13. This means that the primary energy of UHECR may be overestimated when using the HiRes photon yields. In order to know how much the energy is overestimated, it is necessary to take into account the wavelength dependence of the attenuation of photons in the air (Rayleigh and Mie scattering), the optical filter used, the quantum efficiency of the PMT's and other factors which depend on the wavelength.



Considering only Rayleigh scattering and the optical filter transmission coefficient for the HiRes experiment, we have estimated a change in energy of HiRes events if we use the present results instead of their values. The HiRes result may be overestimated by about 10 % for showers of a distance around 10 km and this value increases as the distance increases. We must evaluate the factor in more detail, by taking into account the seasonal and daily variation of the density, temperature and the Mie scattering at the experimental site, and the reconstructed geometry of each shower track.

## 5 Conclusion

Photon yields have been measured in six wave bands as a function of pressure, for nitrogen and dry air excited by electrons of an average energy of 0.85 MeV. The pressure dependencies of fluorescence decay time were also measured. The results are summarized as follows:

- (1) Nitrogen results: The fluorescence efficiencies at 800 hPa are in good agreement with the results by Kakimoto et al. [6,11] at 337 nm and 358 nm, but are smaller by a factor of 2.8 compared with the values of Davidson and O'Neil [14] at 337, 358 and 380 nm. On the other hand, at 391 nm the present result agrees with theirs.
- (2) Air results : The fluorescence efficiencies at 800 hPa are in good agreement with the previous experiments [6,11,14,16], if we take into account the backgrounds which were not subtracted in Kakimoto et al. However,  $\Phi^\circ$  for 391 nm is smaller, by a factor 3.5, than the measurement of Hirsh et al. [12], provided we use the best fit value of  $p'$  from our experiment.
- (3) The photon yield between 300 nm and 406 nm at 1000 hPa and 20 °C is  $3.734 \pm 0.148$  per meter for an electron of 0.85 MeV. The systematic error is 13.2 %, with the main contribution relating to the collection efficiency of the PMT. The photon yield is proportional to  $\frac{dE}{dx}$ , and its density and temperature dependence is given by Eq.(18).
- (4) The photon yield between 300 nm and 406 nm used by the HiRes experiment is about 13 % smaller than determined by the present experiment. If we take into account the wavelength dependence of Rayleigh scattering and the transmission coefficient of the HiRes filter, the primary energies of UHECRs based on their photon yield is probably overestimated. The numerical factor depends on the distance between the shower trajectory and the experimental site.

## Acknowledgements

We acknowledge M.Teshima of ICRR, University of Tokyo, for helping us to prepare the experimental equipment and J.Hayami of Fukui University of Technology for his kind support for this experiment. We are also grateful to B.Dawson of the University of Adelaide for his improvement of the manuscript and his kind advice. This work is supported in part by the grant-in-aid for scientific research No.12440068 from JSPS (Japan Society for the Promotion of Science).

## References

- [1] R.M. Baltrusaitis et al., Nucl. Instrum. Methods Phys. Res. **A240** (1985) 410.
- [2] T. Abu-Zayyad et al., Proc. 26th Int. Cosmic Ray Conf., Salt Lake City, **5** (1999) 349.
- [3] R. Cester et al., Proc. 27th Int. Cosmic Ray Conf., Hamburg, (2001) 711.
- [4] L. Scarsi et al., Proc. 27th Int. Cosmic Ray Conf., Hamburg (2001) 839.
- [5] A.N. Bunner, Ph.D. thesis (Cornell University) (1967).
- [6] F. Kakimoto, E.C. Loh, M. Nagano, H. Okuno, M. Teshima and S. Ueno, Nucl. Instrum. Methods Phys. Res., **A372** (1996) 244.
- [7] T. Abu-Zayyad et al., Proc. 27th Int. Cosmic Ray Conf., Hamburg (2001) .
- [8] M. Takeda et al., Phys. Rev. Lett. **81** (1998) 1163,
- [9] M. Nagano, K. Kobayakawa and N. Sakaki, Proc. 27th Int. Cosmic Ray Conf., Hamburg (2001) .
- [10] J.W. Elbert, in Proc. of Tokyo Workshop on Techniques for the Study of Extremely High Energy Cosmic Rays, ed. by M. Nagano (ICRR, University of Tokyo), (1993) 232.
- [11] S. Ueno, Master thesis (Tokyo Institute of Technology), (1996) (in Japanese).
- [12] M.N. Hirsh, E. Poss and P.N. Eisner, Phys. Rev. A **1** (1970) 1615.
- [13] A.G. Frodesen, O.S. Skjeggstad and H. Tøfte, “Probability and Statistics in Particle Physics” (Universitetsforlaget, Bergen-Oslo-Tromsø) (1979).
- [14] G. Davidson and R. O’Neil, J. Chem. Phys. **41** (1964) 3946.
- [15] R.M. Sternheimer et al. Phys. Rev. B **26** (1982) 6067.
- [16] P. Hartman, Los Alamos report (1963). (cited from Bunner[5]).

- [17] Z. Cao, private communication.
- [18] Particle Data Group, Phys. Rev. D **66** (2002) 010001.
- [19] *U.S. Standard Atmosphere 1976*, U.S. Government Printing Office (Washington D.C., 1976).